Journal of ELECTRONIC MATERIALS, Vol. 47, No. 7, 2018
https://doi.org/10.1007/s11664-018-6215-8

Application of Chlorophyll as Sensitizer for ZnS Photoanode in a Dye-Sensitized Solar Cell (DSSC)

B.B. PANDA,[1,4] P.K. MAHAPATRA,[2] and M.K. GHOSH[3]

1.—Department of Applied Chemistry, Indira Gandhi Institute of Technology, Sarang, Dhenkanal, Odisha 759146, India. 2.—Department of Chemistry, G.M. University, Sambalpur, Odisha 768004, India. 3.—Department of Chemistry, Palsama College, Deogarh, Odisha 768109, India. 4.—e-mail: binodgcek@gmail.com

Zinc sulphide thin films have been synthesized by the electrodeposition method onto stainless steel substrate followed by dipping in acetone solution of chlorophyll in different time intervals to form photosensitised thin films. The photoelectrochemical parameters of the films have been studied using the photoelectrochemical cell having the cell configuration as follows photoelectrode/NaOH(1 M) + S(1 M) + Na_2S(1 M)/C (graphite). The photoelectrochemical characterization of the semiconductor film and dye-sensitised films has been carried out by measuring current–voltage (I–V) in the dark, power output and photoresponse. The study proves that the conductivity of both ZnS film and dye-sensitised ZnS films are *n*-type. The power output curves illustrate that open circuit voltage (V_{oc}) and short circuit current (I_{sc}) increase from 0.210 V to 0.312 V and from 0.297 mA to 0.533 mA, respectively. The fill factor initially decreases from 0.299 to 0.213 and then increases to 0.297 irregularly whereas efficiency increases from 0.047% to 0.123%. The UV–Vis absorbance spectrum of chlorophyll in acetone shows the presence of chlorophyll. The structural morphology of the ZnS thin films has also been analysed by using x-ray diffraction technique (XRD) and a scanning electron microscope (SEM). The XRD pattern shows the formation of nanocrystalline ZnS thin films of size 65 nm and the SEM images confirm the formation of fibrous film of ZnS. The energy diffraction analysis of x-ray confirms the formation of ZnS thin films.

Key words: SEM, XRD, chlorophyll, DSSC, photoanode, liquid junction, chalcogenides

INTRODUCTION

Rapid population growth and industrialisation with the unavoidable shrinking of fossil fuels are leading to serious energy problems for future generations.[1] So, renewable energy sources are becoming the only alternative to face the energy crisis.[2] In this contest, wind, solar, hydropower, geothermal, biomass and biofuel energies are widely explored all over the world.[3] However, solar energy is believed to be the capable renewable energy source to solve the future demand.[4] The harnessing of solar energy has become easy after the development of solar technologies. The solar technologies developed to date are broadly classified into three generations such as a first generation based on single crystalline semiconductors, a second generation based on inorganic thin films and a third generation being photovoltaic solar cells.[4] Out of these three, the dye-sensitised solar cell (DSSC) is the promising area of the third generation devices, which may satisfy the energy demand of today.[1] So energy research on DSSC has been the main centre of attention of researchers for a few decades.[5] The eco-friendly, easy fabrication and low cost of production, attract researchers to focus their attention in the proposed field.[6]

(Received November 23, 2017; accepted March 9, 2018; published online March 19, 2018)

Conversion of photons to electricity in DSSC starts when the dye molecules catch photons of incident light and use their energy to excite electrons. The dye injects these electrons (e^-) into the bulk of the semiconductor. The redox reaction of the electrolytes causes the electron to move from the counter electrode to the dye molecules. Electrical energy is thus generated which is harvested in dye-sensitised photovoltaic cells.[7] The schematic representation of components and basic working principle of the DSSC is as follows (Fig. 1):

The redox system plays an important role in the photoelectrochemical cell. So selection of redox couples is important. Although ranges of redox systems are being used, the sulphide/polysulphide is the main choice of researchers as sulphide (S^{2-}) ions easily form complexes and generate polysulphide ions (S_n^{2-}).[8] The elementary reactions of the DSSC are as follows:

$$\mathrm{ZnS/Ch} + h\nu \rightarrow \mathrm{ZnS/Ch}^*, \quad \text{(I)}$$

$$\mathrm{ZnS/Ch}^* \rightarrow \mathrm{ZnS/Ch}^+ + e_{cb}, \quad \text{(II)}$$

$$(2n-4)h^+(\mathrm{ZnS/Ch}) + n\mathrm{S}^{2-} \rightarrow \mathrm{ZnS/Ch} + 2\mathrm{S}_n^{2-}, \quad \text{(III)}$$

$$2\mathrm{S}_n^{2-} + (2n-4)\mathrm{e}^- \rightarrow n\mathrm{S}^{2-}. \quad \text{(IV)}$$

Generally the photoanodes, which absorb photons of DSSC, are made up of wide band gap semiconductors and coated with dye molecules.[9] The semiconductor and dye molecules fabricate a heterojunction, and the potential difference of the two semiconducting materials generates an electric field which gives rise to the photoelectric effect and pushes the photogenerated electrons and holes in the reverse direction, for which, optical and electrical properties of DSSC change.[10] At present, substrates like SnO_2 coated glass, ITO glass, FTO glass, steel, etc., are being used as substrate to deposit semiconducting materials for fabrication of a thin film semiconductor photoelectrode.[11–13] So far as fabrication is concerned, various methods have been proposed for fabrications of thin films like the SILAR (selective ionic layer adsorption and reaction) method,[14] chemical bath deposition (CBD) and dip coating techniques,[15] ultrasonic spraying,[16] the electrodeposition method,[17] hydrothermal synthesis,[18] chemical vapour deposition (CVD) and the sputtering method.[19,20] The thin films semiconductors can be sensitised by coating with dyes. Attempts have been made for a long time to explore the possibility of dye sensitisation with chlorophyll extracted from the bryophyte *Hyophila involuta*, spinach, pPorphyrin and N 719 dye, a natural dye in PEC solar cells.[21–25] Thimol blue has also been used as a sensitizer on PEC solar cell.[26] Herein, zinc sulfide (ZnS) is selected as the photoelectrode as it is an important II–VI semiconducting material. It is a nontoxic low cost chemical and has better chemical stability as compared to other chalcogenides.[27] The ZnS facilitates the incident photons of high energy to arrive at the window-absorber junction, improving the blue response of the photovoltaic cells, which provides better performance of the PEC cell.[28] Zinc sulphide thin film coatings have broad application in the optical and microelectronic industries due to a high refractive index, high effective dielectric constant and wide wavelength pass bands.[20,29] The optoelectronic properties of ZnS are suitable for the use in light-emitting diodes, electroluminescence, and phosphorescence devices.[30] The electrodeposition method has been employed to fabricate the nontoxic thin film of ZnS on steel substrate. Then the semiconductor has been sensitised using chlorophyll. The photoelectrochemical performance has been studied and deposition time has been optimised.

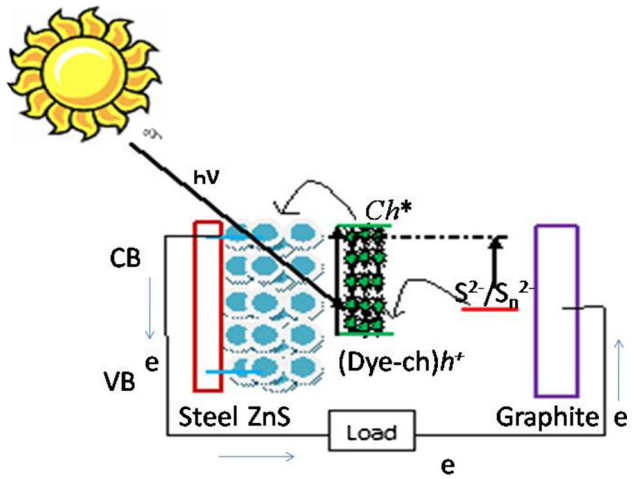

Fig. 1. Schematic representation of components and basic working principle of the DSSC.

EXPERIMENTAL DETAILS

Materials

All chemicals such as zinc sulphate heptahydrate, sodium sulphide, acetone, sodium hydroxide, sulphur, and hydrochloric acid employed for the deposition of thin film are of analytical grade. Double distilled water has been used in all experiments for the preparation of solutions.

Electrolyte Preparation

The sulphide/polysulphide $\left(\mathrm{S}^{2-}/\mathrm{S}_n^{2-}\right)$ redox electrolytes have been used in the photoelectrochemical cell, which were prepared by mixing 1 M NaOH, 1 M Na_2S and 1 M S. The mixture solution was then stirred by magnetic stirrer for 1 h to get a homogenous solution.

Sensitizer Preparation

The chlorophyll is collected from the leaves of the marigold (*Tagetes patula*) plant. The sample was cleaned three times in double distilled water to remove unwanted materials and then dried at 60°C in an oven for 24 h. The dry sample was then ground using mortar and pestle and dissolved in acetone. The solution was then centrifuged to get the required chlorophyll. It was kept at 4°C for further use.

Electrode Preparation

First, 50 ml (0.1 M) of zinc sulphate heptahydrate solution was placed in a 100 ml beaker. Then the steel substrate (2 cm × 2 cm) and a zinc plate (0.5 cm × 0.5 cm) were dipped separating at a distance of 2 cm. Electric current of 2 mA was then passed through a steel substrate (cathode) and a zinc plate (anode) for 2 h to deposit zinc on the substrate. The deposited zinc on steel substrate was then anodised by dipping it in 50 ml of 0.1 m Na_2S by passing current of 2 mA for 2 h using platinum wire as the cathode to obtain the desired ZnS thin film. The thin film semiconductor deposited on steel substrate was then sensitised by dipping in 10 ml chlorophyll solution in acetone. The ZnS thin films were dipped in chlorophyll dye for different durations of time such as 2 h, 4 h, 6 h and 8 h, and; thus, the dipping time was optimised for use of the sensitized thin film for PEC cells.

Fabrication of Solar Cells

The chlorophyll-sensitized solar cells constructed was as

steel/ZnS/sensitizer/ electrolyte $\left(S^{2-}/S_n^{2-}\right)$/

counter electrode (graphite).

UV–Vis Spectroscopy

The UV–Vis spectrum of the chlorophyll-acetone solution was obtained using the double beam UV–Vis spectrophotometer-2202 (systronics) in the range of 350–1000 nm to study the absorbance of chlorophyll.

Structural and Morphological Study

The x-ray diffraction measurements (XRD) were performed on a Siemens (Cheshire, UK) D5000 x-ray diffractometer equipped with CuKα radiation source (λ = 1.5406 Å) at 40 kV and 30 mA with a standard monochromator equipped with a Ni filter, in the range of 10°–80°, using the step size 0:013° and time step 13.6 s. SEM analyses were performed by using a Hitachi S-3000N scanning electron microscope operated at 10 kV.

Characterizations of Liquid Junction Solar Cells

The dark I–V characteristics of DSSCs were studied using two multimeters, and the ideality factors were calculated from the following equations[1,2]:

$$I = I_0\left(e^{\frac{eV}{n_d kT}} - 1\right), \tag{1}$$

$$V_{oc} = \frac{n_l kT}{q} \ln \frac{I_{sc}}{I_o}. \tag{2}$$

I–V characteristics of the DSSCs under 40 mW/cm^{-2} illuminations were studied with a 100 W tungsten bulb using a Lux meter and a multimeter. The short circuit current, open circuit voltage, fill factor (ff), and energy conversion efficiency were calculated using the following equations:

$$\text{ff} = \frac{I_m \times V_m}{V_{oc} \times I_{sc}}, \tag{3}$$

$$\eta = \frac{I_m \times V_m}{P_{input}}. \tag{4}$$

The shunt resistance and series resistance were measured from the equations given below:

$$\left(\frac{\partial I}{\partial V}\right)_{V=0} \cong \frac{1}{R_{sh}}, \tag{5}$$

$$\left(\frac{\partial I}{\partial V}\right)_{I=0} \cong \frac{1}{R_s}. \tag{6}$$

Here, the V_{oc} = open circuit voltage, I_{sc} = short circuit current density, η = energy conversion efficiency P_{input} = total incident power density R_{sh} = shunt resistance, R_s = series resistance, n_d = Ideality factor in dark and n_l = Ideality factor in light.

RESULTS AND DISCUSSION

Absorption Spectroscopy

Figure 2 shows the absorption spectrum of chlorophyll solution in acetone in the wavelength range of 350–1000 nm. The spectrum shows two distinct peaks at 440 nm and 660 nm. The spectrum is attributed to chlorophyll, and the absorption results are in reasonable agreement with that of Amao and Komori.[31] Thus, chlorophyll dye is useful for sensitisation in DSSC. It can be seen that there are two maxima in the absorbance spectrum of chlorophyll. The absorption observed at 440 nm represents $\pi \rightarrow \pi$ transition and 660 nm represents the $n \rightarrow n$ transition.[21]

X-ray Diffraction Spectroscopy

The electrodeposited ZnS thin film has been characterized with x-ray diffraction (XRD). Figure 3 shows four peaks at 36.45°, 39.17°, 43.38° and

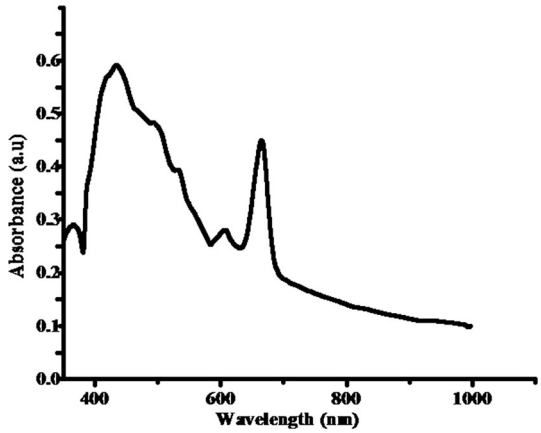

Fig. 2. Absorption spectrum of chlorophyll extract in acetone solution.

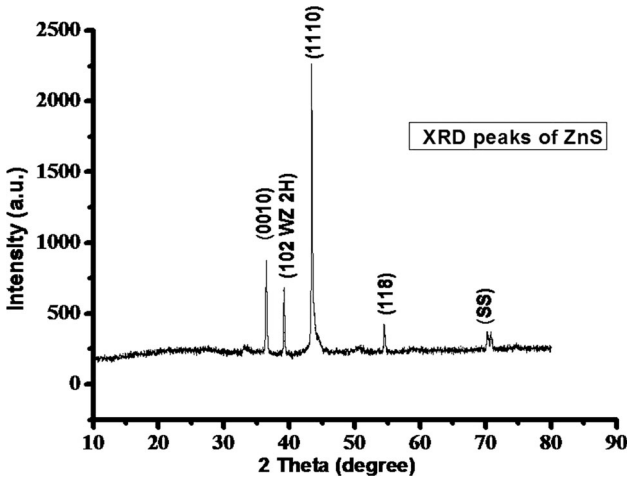

Fig. 3. XRD pattern of ZnS thin film prepared by the electrodeposition method.

54.43° (According to JCPDS FILE NO. 39-1363).[32] The peak at 43.43° is prominent, which indicates the most crystalline nature of the thin film with polycrystalline hexagonal wurtzite mixed structure, however the WZ 8H phase is predominant. The hexagonal structure is preferable for solar cell applications.[33] The crystal size of the thin film has been calculated using Debye Sherrer's formula (Eq. 7)[34]:

$$D = \frac{k\lambda}{\beta \cos\theta}, \tag{7}$$

where D is the crystal size, k is 0.94, λ is the x-ray wavelength (1.54060 Å), β is the full width at half maximum in radians, and θ is Bragg's angle.

The lattice parameters have also been calculated using the relation (8) and found to be $a = 8.77 = b$ and $c = 24.65$. Similar results have been reported by Lokhande and the group.[32] Besides this, other physical parameters of the nanocrystalline thin film have been calculated using the following relation (8, 9 and 10) and are reported in Table I.

$$\frac{1}{d^2} = \frac{4(l^2 + hl + k^2)}{3a^2} + \frac{l^2}{c^2} \tag{8}$$

$$E_{\text{str}} = \frac{\beta \cot}{4} \tag{9}$$

$$\delta = \frac{1}{D^2} \tag{10}$$

Morphology

A scanning electron microscope has been used to study morphology of the surface film.[32] Figure 4 shows SEM images of the semiconductor films in the magnification range of 6000 and 50,000. The image establishes the formation of nanometer-scale-sized fibres. The sizes of the observed fibres are dissimilar. The average length and diameter of the fibres have been measured and found to be of about 0.4–0.8 μm length and of about 80–90 nm diameter. The morphology provides a path for easier electron transport than percolation through the random spherical nanoparticles. This may be accredited to increased electron diffusion length with better photochemistry.[32]

Composition Analysis

The typical EDAX spectrum of electro-deposited thin films is shown in Fig. 5. The elemental analysis shows the presence of Zinc (Zn) and sulphur (S) along with some other elements. In the spectra a carbon peak is observed due to the substrate holder and an oxygen peak might be due to the partial oxidation of film. The relative average atomic percentage ratio of Zn:S is about 1:1 for the films, indicating the formation of film with stoichiometric composition.

Thickness Measurement

The average thickness of the deposited semiconductor thin film has been measured gravimetrically.[35] The thickness of the ZnS films has been found to be 80 μm.

Conductivity and I–V Characteristics

The dark I–V curve is one of the basic parameters for solar cells characterisation. The results have importance for the understanding about the devices. The dark I–V curve is influenced by mostly significant series resistance and front contact-specific resistance. Figure 6 shows the dark I–V curves of the fabricated cell under forward and reverse bias of ZnS and chlorophyll dye sensitized ZnS thin films semiconductors at room temperature. The

Table I. Structural pParameters of ZnS thin film deposited on steel substrate by the electrodeposition method

2θ	θ	(*hkl*) planes	FWHM	d-spacing	Crystal size (nm)	Strain	Dislocation density ($\delta = 1/D^2$)
36.456	18.228	(0010)	0.134	2.465	65.310	1.8×10^{-3}	2.34×10^{-4}
39.175	19.588	(102WZ2H)	0.134	2.300	65.840	1.6×10^{-3}	2.3×10^{-4}
43.385	21.692	(1110)	0.167	2.086	53.520	1.8×10^{-3}	2.49×10^{-4}
54.409	27.205	(118)	0.134	1.895	69.790	1.1×10^{-3}	2.05×10^{-4}

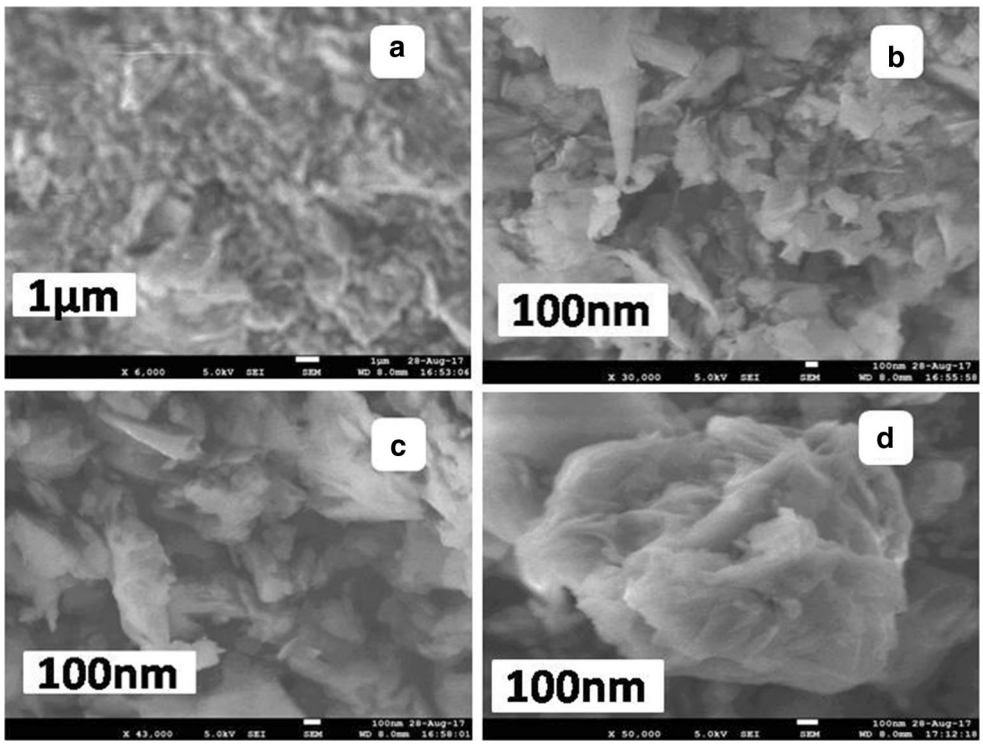

Fig. 4. Top view of scanning electron microscope image (SEM) of a ZnS thin film prepared by the electrodeposition method on steel substrate in the magnification range of (a) 6000 (b) 30,000 (c) 43,000, and (d) 50,000.

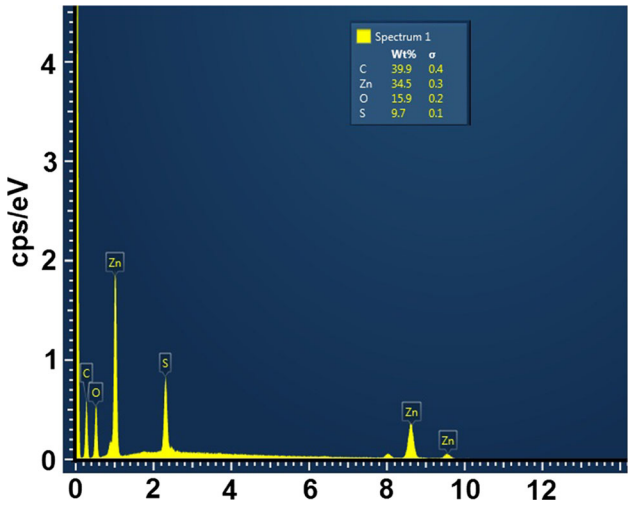

Fig. 5. EDAX spectrum of a ZnS thin film prepared by the electrodeposition method.

nonsymmetrical nature of the graph indicates the rectifying behaviour of the photoelectrochemical (PEC) cells and formation of a *p*–*n* junction in the cells.[36] Here, the photodiode may involve the creation of electron–hole [e–h] pairs by the absorption of incident light having energy greater than the band gap of the semiconductor, splitting and transport of the e–h pairs by the internal electric field, and the interaction of current with the external circuit to generate an output signal. The I–V characteristics of a photodiode in a dark environment are similar to those of a normal rectifying diode. If the *p*–*n* junction does not form, the generated e–h pairs will exhibit an ohmic character in the I–V curve and change the resistance.[14,37]

The behaviour of a semiconductor/electrolyte interface has been studied using the current–voltage relations under illumination of photoelectrode. The current–voltage plot (Fig. 7) shows

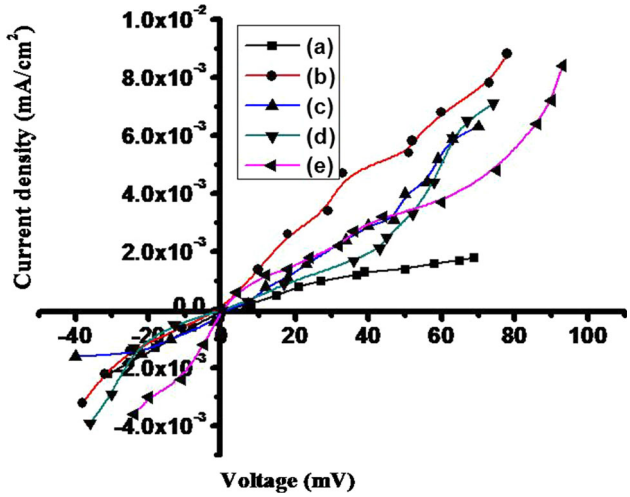

Fig. 6. Dark I–V curve of (a) ZnS thin film and chlorophyll sensitized ZnS thin films photoanodes for (b) 2 h, (c) 4 h, (d) 6 h, and (e) 8 h.

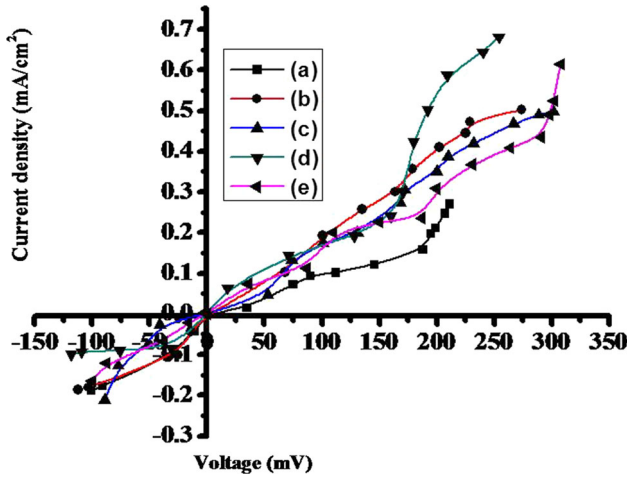

Fig. 7. Light I–V curve of (a) ZnS thin film and chlorophyll sensitized ZnS thin films photoanodes for (b) 2 h, (c) 4 h, (d) 6 h, and (e) 8 h.

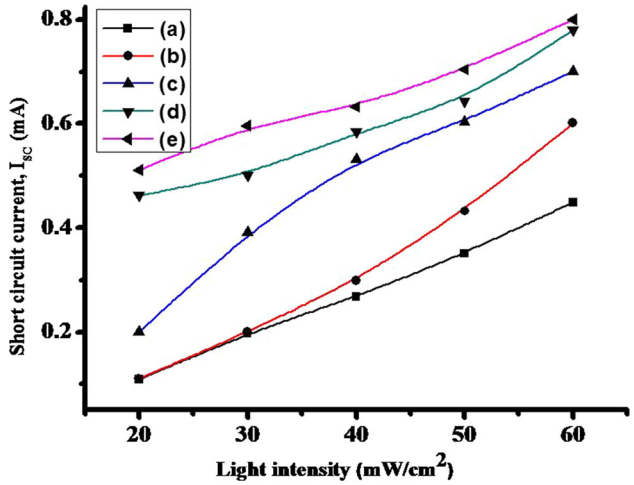

Fig. 8. Variation of I_{SC} versus light intensity curve of (a) ZnS thin film and chlorophyll sensitized ZnS thin films photoanodes for (b) 2 h, (c) 4 h, (d) 6 h, and (e) 8 h.

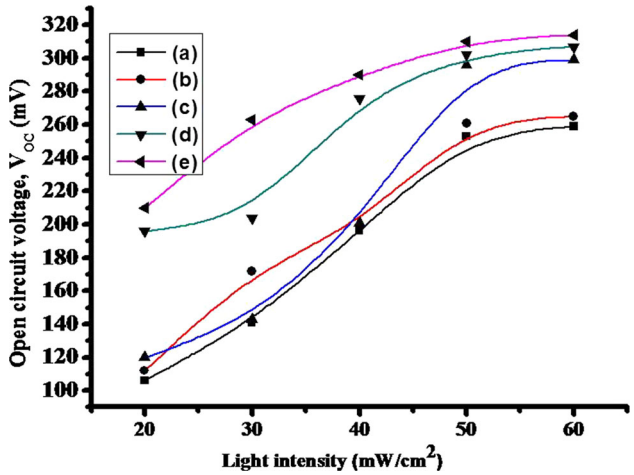

Fig. 9. Variation of V_{oc} versus light intensity curve of (a) ZnS thin film and chlorophyll sensitized ZnS thin films photoanodes for (b) 2 h, (c) 4 h, (d) 6 h, and (e) 8 h.

that, under illumination, the I–V curves are shifted anticlockwise, which indicates that light can be converted to electricity in the cell.[37] The sweep in current after light illumination is attributed to the generation of free electron–hole pairs in the conduction and valence band by the incident photons. The photon energy breaks a few covalent bonds, enhancing charge carrier concentration both in the valence band and conduction band by generating free holes and electrons, respectively.[38]

The variation of short circuit current and open circuit voltage against light intensity has been studied to understand the photoresponse of the photoelectrochemical cells using synthesised electrodes and chlorophyll sensitised electrodes towards light. Figure 8 shows the variation of short circuit current against light intensity. The almost straight line variation of short circuit current against light intensity indicates that the (ZnS) photoelectrode–$\left(S^{2-}/S_n^{2-}\right)$ electrolyte interface may be the representation of a Schottky barrier solar cell.[39] But saturation of open circuit voltage (V_{oc}) is observed in the curve of open circuit voltage against light intensity (Fig. 9) which illustrates the saturation of the electrode–electrolyte interface, charge transfer and non-equilibrium dispersion of electrons and holes in the space charge area of the photoelectrode.[27]

Power Output Studies

Figure 10 shows the photovoltaic power output of the dye-sensitised solar cell under light illumination of 40 mW/cm^2 over the electrode area of 1.5 cm^2, from which maximum power generated can be measured from the biggest rectangle formed inside the curves. The parameters calculated using the

relation (3, 4, 5, and 6) is given in Table II. The results show that the J_{sc}, V_{oc} and efficiency are continuously increasing with the increase of deposition time. The increase of J_{sc} and V_{oc} might be due to the increase of electron transport, electron density and electron life time. The increase of efficiencies might be due to the increase of J_{sc}.[40] The data show that the conversion efficiency of solar energy to electricity in DSSC is 0.12%. The efficiency reported by Hankare[27] was 0.53%. It might be the cause of higher illumination area. Another parameter for solar cell characterisation is fill factor (FF). In solar cells the P_{max} is related to fill factor. The fill factor for DSSC is low due to parasitic resistance (R_s, R_{sh}) and the charge recombination at semiconductor/electrolyte interface. The series resistance reduces the fill factor and, hence, the efficiency of the solar cell. The series resistance developed in the circuit of solar cells might be from the migration of electrons in the semiconductor and the dispersion of ions in the electrolyte, the resistance at the interface between the semiconductor and the transparent conductive film, and the resistance of the metal contacts. The shunt resistance developed may be due to the crystal defects, which provide an alternate pathway for electrons causing power loss. Thus, broadly it can be stated that, a small series resistance and a large R_{sh} resistance are considered to be helpful to realize a high fill factor.

The low fill factor in our ZnS solar cells likely implies the severe charge recombination at the semiconductor surface and/or at the semiconductor and electrolyte interface. The low fill factor has also been reported by Otsuka et al.[41] The fill factors in all cases do not change appreciably. Similar trends have also been reported by a number of workers.[1,24,40] However, variation of fill factors might be the reason for the variation of series resistance and shunt resistance. It is a low-resistance connection between two points in an electric circuit that form an alternative path for a portion of the current. Shunt resistance (R_{sh}) provides an alternative way for light generated photocurrent which is responsible for power loss in dye-sensitised solar cells. Such

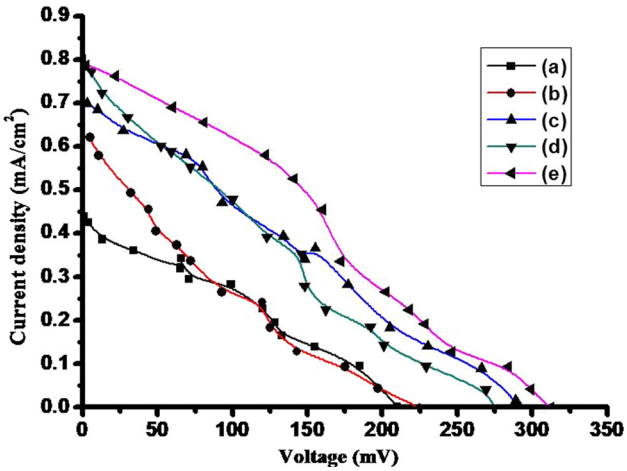

Fig. 10. Power output characteristics curve of (a) ZnS thin film and chlorophyll-sensitized ZnS thin films photoanodes for (b) 2 h, (c) 4 h, (d) 6 h, and (e) 8 h.

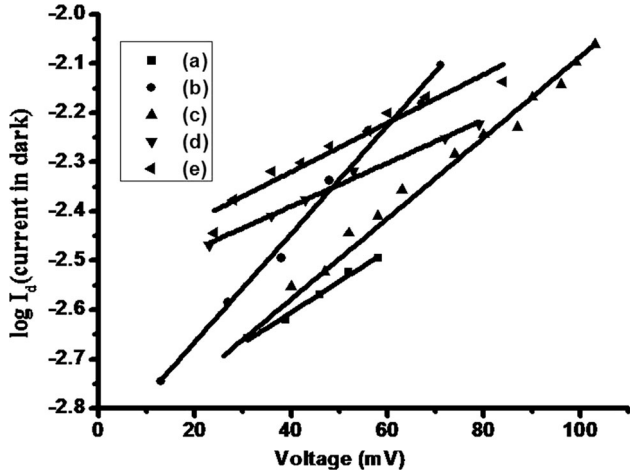

Fig. 11. Determination of junction ideality factor in the dark of (a) ZnS thin film and chlorophyll-sensitized ZnS thin films photoanodes for (b) 2 h, (c) 4 h, (d) 6 h, and (e) 8 h.

Table II. Electrical parameters for the electrodeposited (a) ZnS and chlorophyll sensitized electrodes by dipping in chlorophyll solution in acetone for (b) 2 h (c) 4 h (d) 6 h, and (e) 8 h prepared on steel substrates based on PEC cells with IM (Na_2S, S, NaOH) redox electrolyte at a light intensity of 40 mW/cm² shown in Fig. 10

Electrode	J_{sc} (mA/cm²)	V_{oc} (V)	FF	Efficiency (%)	Ideality factor in dark (I_d)	Ideality factor in light (I_l)	R_s (Ω cm²)	R_{sh} (Ω cm²)
ZnS	0.297	0.210	0.299	0.047	1.750	3.800	291.262	962.620
2 h	0.400	0.227	0.213	0.048	5.400	9.400	688.073	401.665
4 h	0.463	0.290	0.283	0.095	2.420	6.400	900.000	718.579
6 h	0.520	0.275	0.241	0.086	2.320	6.100	1285.714	489.573
8 h	0.533	0.312	0.297	0.123	1.080	4.300	229.008	862.500

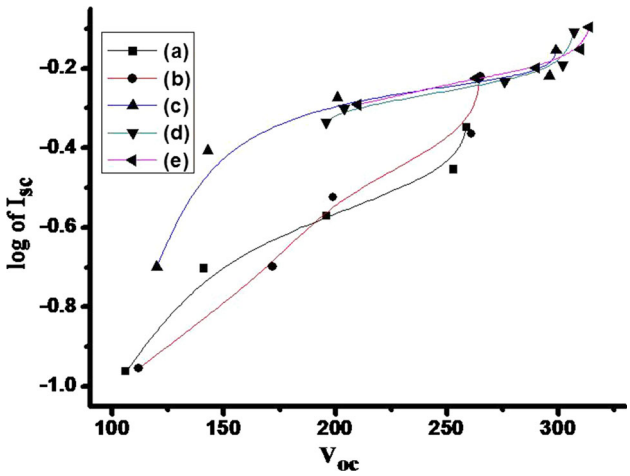

Fig. 12. Determination of junction ideality factor in light of (a) ZnS thin film and chlorophyll-sensitized ZnS thin films photoanodes for (b) 2 h, (c) 4 h, (d) 6 h, and (e) 8 h.

a diversion reduces the amount of current following through the solar cell and thereby reduces the voltage from the cell. Series resistance can drastically reduce the output power as a R_s value of only 5 Ω can reduce the power output by 30%. The higher R_{sh} and low R_s might be the cause of high fill factor (0.299) in ZnS thin films. After sensitisation in 2 h, 4 h and 8 h, the fill factor is increasing (0.213, 0.241, and 0.297). It might be the reason for the increase of R_{sh}. In 6 h sensitisation the fill factor decreases due to low R_{sh}.

The ideality factor of a diode junction is an important parameter in order to study the ideality of a diode (how closely the diode follows the ideal diode equation). This is a fundamental parameter to describe the diode junction and electrical behaviour of solar cells.[42] The efficiency of a solar cell is very much influenced by the generation-recombination of e–h pairs on the electrode–electrolyte, tunneling, etc., that can be predicted by the ideality factor values which depend on temperature and the applied voltage.[43] In particulars the ideality factor plays an important role in voltage across the device. The ideality factor approaches to one at high voltage, when the surfaces and the bulk regions dominate the recombination in the device. But at lower voltages, in reverse cases the ideality factor is more. Recombination is improved by defects. The higher the defects, the higher are the space charge recombinations. The deviation of ideality factor from one attributes the occurrence of unusual recombination mechanisms.[44] The higher value of light ideality factor (n_1) is suggestive of the effect of series resistance and the carrier recombination at the semiconductor–electrolyte interface.[45] The high ideality factor may also be the cause of inhomogeneities of film thickness, non-uniformity of the interfacial charges and the effect of the series resistance (R_s).[46] In the present study, the ideality factors in dark and light have been measured from the plot of log I_d vs applied voltage and log I_{sc} vs V_{oc} (Figs. 11 and 12) using Eqs. 1 and 2 (Table II). The results show that initially the dark and light ideality factors are increasing due to increase of R_s however the values are decreasing due to decrease of R_s.[38]

CONCLUSION

ZnS wide gap semiconductor has been prepared successfully by the electrodeposition method and sensitised using chlorophyll dye extracted from *Tagetes patula* by dipping at different time intervals. The absorption spectrum of chlorophyll dye shows two prominent peaks at 440 nm, and 660 nm that confirm the extraction. The XRD pattern confirms the formation of nanocrystalline ZnS thin film. The results show that chlorophyll sensitizer produced a high power conversion efficiency of tenfold as compared to a simple electrode. This implies that wide band gap semiconductors can be sensitised using chlorophyll dye for the use in DSSCs.

REFERENCES

1. F. Bella, C. Gerbaldi, C. Barolo, and M. Gratzel, *Chem. Soc. Rev.* 44, 3431 (2015).
2. T.C. Kandpal and L. Broman, *Renew. Sustain. Energy Rev.* 34, 300 (2014).
3. G.D.A. Jebaselvi and S. Paramasivam, *Renew. Sustain. Energy Rev.* 28, 625 (2013).
4. H.K. Jun, M.A. Careem, and A.K. Arof, *Renew. Sustain. Energy Rev.* 22, 148 (2013).
5. A. Hagfeldt, *AMBIO* 41, 151 (2012).
6. V. Shanmugam, S. Manoharan, S. Anandan, and R. Murugan, *Spectrochim. Acta Part A: Mol. Biomol. Spectrosc.* 104, 35 (2013).
7. C.-L. Lee, W.-H. Lee, and C.-H. Yang, *Int. J. Photoenergy*, Article ID 250397 (2013).
8. V. Chakrapani, D. Baker, and P.V. Kamat, *J. Am. Chem. Soc.* 133, 9607 (2011).
9. A. Jena, S.P. Mohanty, P. Kumar, J. Naduvath, V. Gondane, P. Lekha, J. Das, H.K. Narula, S. Mallick, and P. Bhargava, *Trans. Ind. Ceram. Soc.* 71, 1 (2012).
10. H. Pan, *Renew. Sustain. Energy Rev.* 57, 584 (2016).
11. Y. Zhou, M. Yang, W. Wu, A.L. Vasiliev, K. Zhu, and N.P. Padture, *J. Mater. Chem. A* 3, 8178 (2015).
12. R.G. Lua, J.E. Garcıa, D.P. Martınez, M.T.S. Nair, J. Campos, and P.K. Nair, *ECS J. Solid State Sci. Technol.* 4, Q9 (2015).
13. Y.L. Lee, C.F. Chi, and S.Y. Liau, *Chem. Mater.* 22, 922 (2010).
14. J. Henry, K. Mohanraj, and G. Sivakumar, *J. Asian Ceram. Soc.* 4, 81 (2016).
15. S.H. Chaki, M.P. Deshpande, and J.P. Tailor, *Thin Solid Films* 550, 291 (2014).
16. C.H. Hsu, L.C. Chen, and X. Zhang, *Materials* 7, 1261 (2014).
17. P. Wang, H. Wu, Y. Tang, R. Amal, and Y.H. Ng, *J. Phys. Chem. C* 119, 26275 (2015).
18. A.M. Telia, G.J. Navathea, D.S. Patil, P.R. Jadhava, S.B. Patil, T.D. Dongale, M.M. Karanjkarc, J.C. Shin and P.S. Patil, *Sustain Energy Fuels*. 1, 377 (2017). https://doi.org/10.1039/C6SE00016A.
19. H.J. Snaith and C. Ducati, *Nano Lett.* 10, 1259 (2010).
20. H. Abdullah, N. Saadah, and S. Shaari, *World Appl. Sci. J.* 19, 1087 (2012).

21. H.C. Hassan, Z.H. Z. Abidin, F.I. Chowdhury, and A.K. Arof, *Int. J. Photoenergy*, Article ID 3685210 (2016). http://dx.doi.org/10.1155/2016/3685210.
22. R. Syafinara, N. Gomesha, M. Irwantoa, M. Fareqa, and Y.M. Irwan, *Energy Procedia* 79, 896 (2015).
23. L.L. Li and E.W.G. Diau, *Chem. Soc. Rev.* 42, 291 (2013).
24. X. YaoMing, W. JiHuai, C. CunXi, C. Yuan, Y. GenTian, L. JianMing, H. MiaoLiang, F. LeQing, and L. Zhang, *Chin. Sci. Bull.* 57, 2329 (2012).
25. G. Calogero, G. Di Marco, S. Caramori, S. Cazzanti, R. Argazzic, and C.A. Bignozzi, *Energy Environ. Sci.* 2, 1162 (2009).
26. P.K. Mahapatra and B.B. Panda, *Chalcogenide Lett.* 7, 477 (2010).
27. P.P. Hankare, P.A. Chate, and D.J. Sathe, *J. Alloys Compd.* 487, 367 (2009).
28. R. Sharma, B.P. Chandra, and D.P. Bisen, *Chalcogenide Lett.* 6, 339 (2009).
29. J. Hasanzadeh, A. Taherkhani, and M. Ghorbani, *Chin. J. Phys.* 51, 540 (2013).
30. S.H. Deulkara, C.H. Bhosalea, and M. Sharonb, *J. Phys. Solids* 65, 1879 (2004).
31. Y. Amao and T. Komori, *Biosens. Bioelectron.* 19, 843 (2004).
32. A.B. Bhalerao, C.D. Lokhande, and B.G. Wagh, *IEEE Trans. Nanotechnol.* 12, 996 (2013).
33. P. Kumar, A. Misra, D. Kumar, N. Dhama, T.P. Sharma, and P.N. Dixit, *Opt. Mater.* 27, 261 (2004).
34. B.B. Panda, B. Sharma, and R.K. Rana, *Mater. Sci. Pol.* 34, 446 (2016).
35. P.K. Mahapatra and B.B. Panda, *Int. J. Thin Films Sci. Technol.* 4, 45 (2015).
36. R.M. Mane, S.S. Mali, V.B. Ghanwat, V.V. Kondalkar, K.V. Khot, S.R. Mane, D.B. Shinde, P.S. Patil, and P.N. Bhosale, *Mater. Today Proc.* 2, 1458 (2015).
37. A.A. Yadav and E.U. Masumdar, *J. Alloys Compd.* 509, 5394 (2011).
38. N.P. Husea, A.S. Divea, K.P. Gattub, and R. Sharma, *Mater. Sci. Semicond. Process.* 67, 62 (2017).
39. K. Rajeshwar, L. Thomson, P. Singh, R.C. Kainthala, and K.L. Chopra, *J. Electrochem. Soc.* 128, 1744 (1981).
40. Y. Duan, N. Fu, Q. Liu, Y. Fang, X. Zhou, J. Zhang, and Y. Lin, *J. Phys. Chem. C* 116, 8888 (2012).
41. A. Otsuka, K. Funabiki, N. Sugiyama, and T. Yoshida, *Chem. Lett.* 35, 666 (2006).
42. K. Alfaramawi, *Dig. J. Nanomater. Biostruct.* 5, 933 (2010).
43. J. Verschraegen, M. Burgelman, and J. Penndorf, *Thin Solid Films* 307, 480 (2005).
44. A.D.A. Buba, E.O. Ajala, and D.O. Samson, *Asian J. Sci. Technol.* 6, 1146 (2015).
45. S.M. Pawar, A.V. Moholkar, K.Y. Rajpure, and C.H. Bhosale, *Sol. Energy Mater. Sol. Cells* 92, 45 (2008).
46. S. Aydogan and O. Gullu, *Microelectron. Eng.* 87, 187 (2010).